Journal of Solid State Chemistry 193 (2012) 142–146

Contents lists available at SciVerse ScienceDirect

Journal of Solid State Chemistry

journal homepage: www.elsevier.com/locate/jssc

Synthesis and characterization of Bi-doped Mg_2Si thermoelectric materials

S. Fiameni *, S. Battiston, S. Boldrini, A. Famengo, F. Agresti, S. Barison, M. Fabrizio

CNR - IENI, Corso Stati Uniti 4, 35127 Padova, Italy

ARTICLE INFO

Available online 15 May 2012

Keywords:
Thermoelectric
Silicides
Carbon nanohorn

ABSTRACT

The Mg_2Si-based alloys are promising candidates for thermoelectric energy conversion for the middle high range of temperature. They are very attractive as they could replace lead-based compounds due to their low cost and non toxicity. They could also result in thermoelectric generator weight reduction (a key feature for the automotive application field). The high value of thermal conductivity of the silicide-based materials could be reduced by increasing the phonon scattering in the presence of nanosized crystalline grains without heavily interfering with the electrical conductivity of the thermoelectric material.

Nanostructured materials were obtained under inert atmosphere through ball milling, thermal treatment and spark plasma sintering processes. In particular, the role of several bismuth doping amounts in Mg_2Si were investigated (Mg_2Si:Bi = 1:x for x = 0.01, 0.02 and 0.04 M ratio). The morphology, the composition and the structure of the samples were characterized by FE-SEM, EDS and XRD analyses after each process step. Moreover, the Seebeck coefficient analyses at high temperature and the electrical and thermal conductivity of the samples are presented in this work. The nanostructuring processes were affect by the MgO amount increase which influenced the thermoelectric properties of the samples mainly by reducing the electrical conductivity.

With the aim of further increasing the scattering phenomena by interface or boundary effect, carbon nanostructures named Single Wall Carbon Nanohorns were added to the Mg_2Si in order to produce a nanocomposite material. The influence of the nanostructured filler on the thermoelectric material properties is also discussed.

1. Introduction

The thermoelectric generators (TEGs) are solid-state devices with no moving parts, noiseless, reliable and scalable, and they are good candidates for obtaining small sized application for distributed power generation [1]. At present, TEG devices are mainly employed for converting thermal energy into electrical energy in aerospatial and military applications but are currently studied for automotive applications.

In this direction many car industries are making efforts in order to couple TEGs to combustion engines for improving the fuel efficiency exploiting the exhaust stream heat recovery [2,3] which correspond roughly to 80% of fuel energy in the conventional combustion engines. Since the amount of fuel used for transportation is a large part of the world energy use, even a small percentage improvement in efficiency could have a great impact from the environmental and economic point of view.

The low efficiency of these materials for energy production does not permit them to be cost effective for most applications [4,5]. However, a great interest in thermoelectrics has begun in the mid-1990s when theoretical predictions suggested that thermoelectric efficiency could be greatly enhanced through nanostructural engineering, which led to experimental efforts to demonstrate the proof of principle and to find high-efficiency materials.

For useful applications the thermoelectric materials require low thermal conductivity κ, high Seebeck coefficient S and high electrical conductivity σ. These parameters determine the figure of merit ZT, which is expressed as $ZT=\sigma S^2 T\kappa^{-1}$, where T is the absolute temperature. Since σ and S are inversely correlated as function of the number of charge carriers, the increase of the figure of merit is quite tricky.

The Mg_2Si-based alloys are promising candidates for thermoelectric energy conversion for the middle-high range of temperature. They are very attractive as they could replace lead-based compounds due to their low cost, non-toxicity [1,2] and abundance of raw materials. They could also result in thermoelectric generator weight reduction (a key feature for the automotive application field [6,7]). P-type Mg_2Si can be produced by doping with Ag and Cu, and n-type can be obtained by doping with Al, Sb and Bi [8–10].

One of the main hindrance to the large scale development of silicide-based devices is their high value of thermal conductivity. This parameter could be reduced by increasing the phonon scattering in the presence of nanosized crystalline grains.

* Corresponding author.
E-mail address: s.fiameni@ieni.cnr.it (S. Fiameni).

0022-4596/$ - see front matter © 2012 Elsevier Inc. All rights reserved.
http://dx.doi.org/10.1016/j.jssc.2012.05.004

This does not heavily interfere with the electrical conductivity of the thermoelectric material [11,12].

The aim of this work is the study of nanostructured silicide thermoelectric materials employing commercial Mg_2Si raw pieces as starting material. This approach was chosen to avoid the difficulties and costs related to the employment of Mg metal powders, in order to plan a large scale production of silicide-based devices.

The role of several bismuth doping amounts (Mg_2Si:Bi = 1:x for x = 0.01, 0.02 and 0.04 M ratio) in Mg_2Si were investigated.

Recently, Gothard et al. [13] introduced small amount of fullerene as phonon scattering centers into TE materials to reduce the thermal conductivity. In order to further explore the effect on thermoelectric properties of carbon nanostructures, Single Wall Carbon Nanohorns (SWCNHs) were added to the Bi-doped Mg_2Si. The SWCNHs [14,15] indeed represent one of the most interesting carbon nanostructures belonging to the thrived nanotube family. A key characteristic is their tendency to group together and form aggregates (spherical clusters or bundles) like dahlia flowers or buds, with overall diameters of tens/hundreds nanometers. In spite of their tiny conical structure, SWCNHs maintain many of the typical properties of carbon nanotubes such as good electrical and thermal conductivities and the easiness of functionalization. Interesting influence of this kind of carbon nanostructures in ceramic composite materials on their morphological shape and functional properties were previously reported [16–18].

2. Experimental

Silicide-based pellets were produced starting from commercial magnesium silicide pieces (99,99%, Alfa Aesar), Bi powder (99,5%, Alfa Aesar) and SWCNHs (Carbonium Srl) with diameter ranging between 50 and 100 nm [19].

The thermal stability of SWCNHs was tested by thermogravimetric analysis (TGA, simultaneous SDT Q600-TA instruments) heating 2 mg of SWCNH powder in an alumina crucible from 30 up to 900 °C at 5 °C min^{-1} under pure N_2 (100 mL min^{-1}). Raw Mg_2Si together with different amounts of Bi were ground under Ar atmosphere in a planetary ball mill (BM) with hexane as dispersion medium (WC jar, 330 rpm for 24 h), to obtain samples with x = 0.01, 0.02 and 0.04, where x is the Bi:Mg_2Si molar ratio. In order to obtain the effective Bi doping of magnesium silicides, the milled powder were pressed and heated at 600 °C for 2 h in Ar flow (3 L min^{-1}). The heating rate was 5 °C min^{-1} whilst, at the end of the treatment, the samples were subject to a free cooling process. Afterwards, the powders were ground again in Ar atmosphere and sintered via Spark Plasma Sintering (SPS) at 800 °C under 60 MPa for 2 min in a graphite die (heating rate of 100 °C min^{-1} and free cooling process). The crystalline phases were revealed by X-ray diffraction (XRD) using a Philips PW 3710 X-ray diffractometer with Bragg–Brentano geometry and a CuK_α source (40 kV, 30 mA). The Rietveld refinement on the XRD profiles has been exploited to obtain information about phase amounts, crystallite sizes and lattice parameters [20].

The morphological and compositional characterizations were performed by Sigma Zeiss Field Emission SEM equipped with Oxford X-Max EDS system.

The thermal diffusivity and the specific heat of the samples were measured by a laser flash thermal diffusivity apparatus (Netzsch LFA 457 MicroFlash®). The thermal conductivity κ was calculated according to the formula $\kappa = a\rho C_p$ where a is the thermal diffusivity, ρ the density and C_p the specific heat of the material. The Seebeck coefficient and the electrical conductivity were measured in the RT to 600 °C temperature range using a custom test apparatus described elsewhere [21]. All measurements were carried out under Ar atmosphere.

3. Results and discussion

In all the samples XRD analysis revealed the presence of free Bi after ball milling treatment. Fig. 1 reports XRD patterns of commercial Mg_2Si and the x = 0.01, 0.02 and 0.04 Bi added Mg_2Si specimens after thermal treatment. Sample with x = 0.02 Bi + SWCNHs presented the same XRD pattern of the one with x = 0.02 Bi. Thermogravimetric analysis was performed on pristine SWCNHs in a temperature range from 30 up to 900 °C under N_2. The calculated weight loss is about 2% of the starting mass demonstrating the carbon nanostructures thermal stability at the employed sintering temperature (800 °C). These results are consistent with the graphene nature of such carbon nanostructures which present a sublimation point above 3500 °C.

For all samples we obtained the Bi doping of magnesium silicides after thermal treatment. Fig. 2(a) shows an example of free Bi peak disappearing after the thermal treatment for sample x = 0.01, leading to a Mg_2Si peak position shift attesting the effective Bi doping of the silicide. This highlighted the need of a thermal treatment of ground powders in order to obtain the Bi doping of Mg_2Si material. The presence of Si related peak in samples after ball milling is due to the partial decomposition of Mg_2Si resulting in MgO formation, observed also in the commercial raw material.

The pattern for x = 0.02, 0.04 and 0.02 + SWCNHs samples also showed the presence of Bi_2Mg_3 as a secondary phase. This is in agreement with the literature data [22].

Fig. 2(b) lists the lattice constant variation of samples depending on the Bi-doping content. The lattice constant increased with increasing of Bi content but showed saturation for Bi content ≥ 0.02 M ratio. This is in agreement with literature data reporting a solubility limit of Bi < 2 at% [23].

The FE-SEM and XRD analyses were carried out after each synthesis step (ball milling, thermal treatment and SPS sintering) for all the samples. The doping amount seemed not to significantly influence the crystallite size, hence the XRD analysis were performed also after thermal and electrical measurements only for the most representative sample, the one with x = 0.02 Bi (Fig. 3). The crystallize size presented a gradual increase after each thermal treatment performed during the synthesis process and during the LFA and

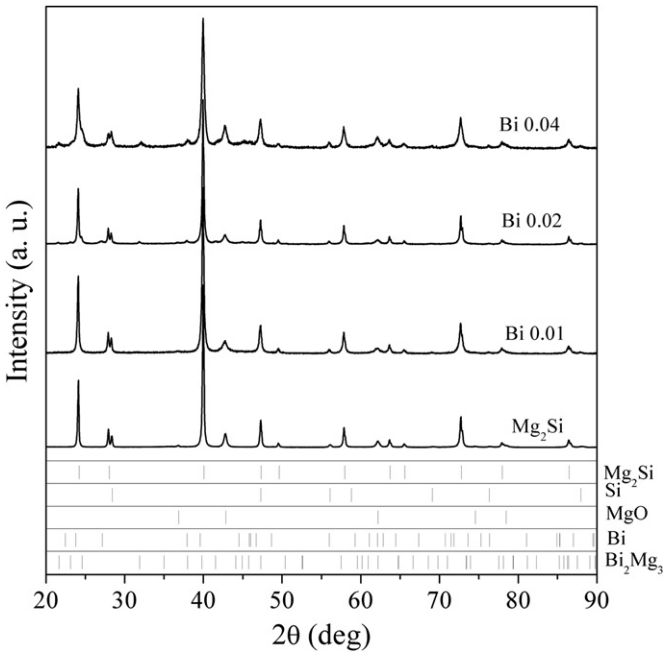

Fig. 1. X-ray diffraction patterns for the samples after ball milling and the thermal treatment at 600 °C for 2 h under inert atmosphere.

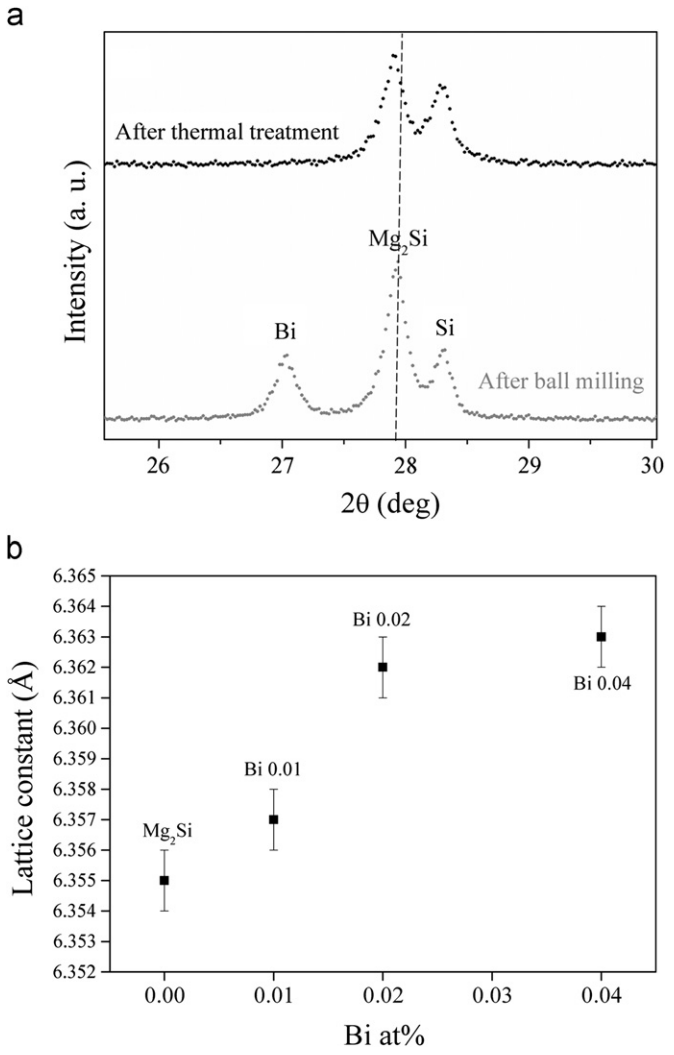

Fig. 2. Particular of the XRD spectrum of $x=0.01$ sample before and after the thermal treatment at 600 °C for 2 h under inert atmosphere (a) and lattice constant as a function of the Bi doping (b).

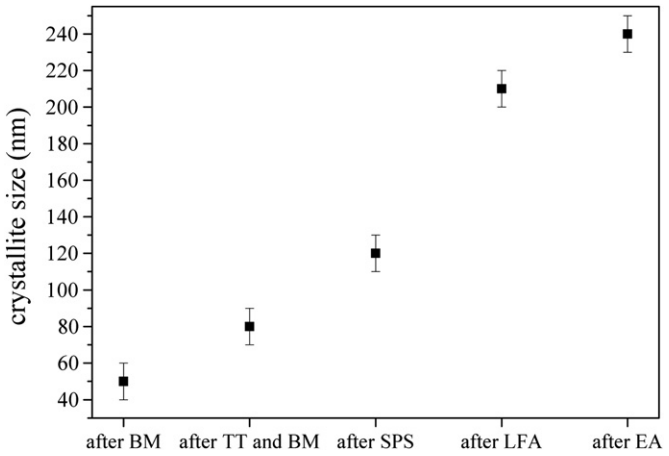

Fig. 3. Crystallite size trend after each synthesis process and after functional analyses.

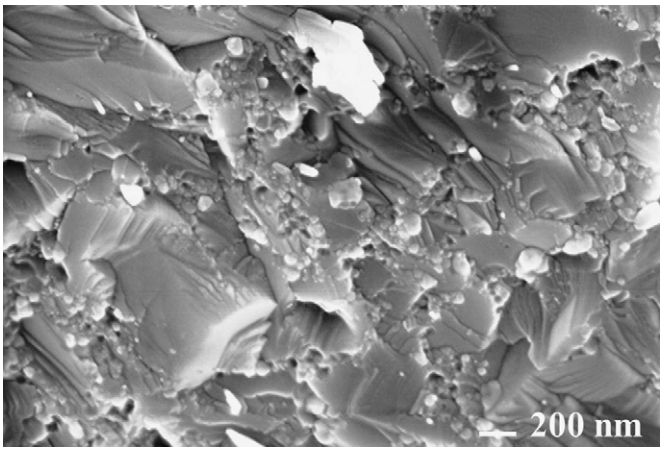

Fig. 4. FE-SEM micrograph after SPS sintering of a fractured doped magnesium silicide pellet with $x=0.02$ Bi.

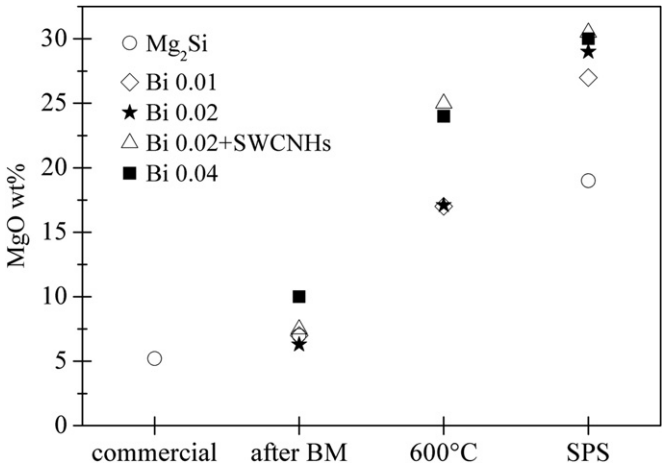

Fig. 5. MgO amount in the commercial material and after the different thermal processes.

electrical analyses (EA). As an example, Fig. 4 reports the SEM image of the sample $x=0.02$ showing the typical morphology of our samples.

This behavior highlights the difficulty to preserve the original grain size in silicide materials since each thermal cycle induced the crystallite size growth. Moreover, XRD analyses showed the MgO increasing in the samples after thermal treatment and SPS (Fig. 5). EDS analyses confirmed the results obtained by XRD analyses. The amount of segregated Si phase ranging from 2 wt% to 8 wt% was consistent with the theoretical values expected from the decomposition of Mg_2Si to MgO and Si.

The temperature dependence of the electrical resistivity of the samples, ρ, is shown in Fig. 6. For all the curves, the electrical resistivity decreased with the temperature, indicating a semiconductor like behavior. As expected, ρ decreased with increasing the Bi doping amount. Furthermore, it is worth highlighting that the presence of SWCNHs further significantly decreased the resistivity, probably due to the conducting nature of aggregated carbon nanostructures. However, all these values are higher with respect to the literature values probably because of the MgO presence, which is detrimental for the electrical conductivity.

The Rietveld refinement of XRD data revealed the presence of 3 wt% of the Bi_2Mg_3 phase in $x=0.04$ sample, whilst in the other samples this phase amount is <1 wt% or absent. Moreover, this sample showed also a resistivity smaller than the $x=0.02$ sample, notwithstanding the solubility limit of Bi <2 at% [23] confirmed also by XRD analyses. This lower resistivity could also be explained by the presence of the metallic phase Bi_2Mg_3.

Seebeck coefficients, listed in Fig. 7, are consistent with the previously reported values [24–28] for the corresponding

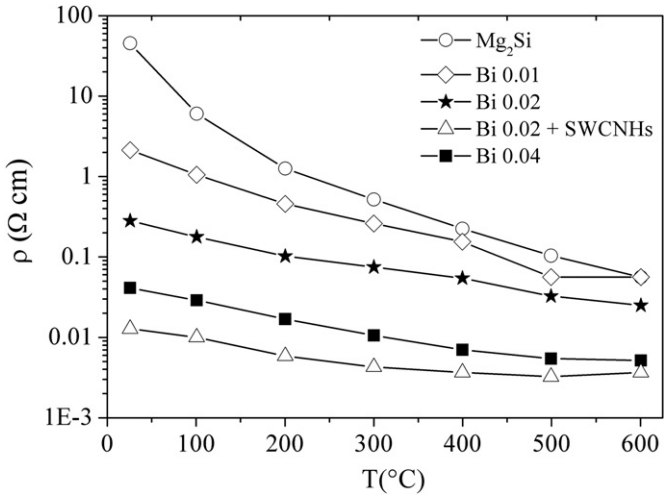

Fig. 6. Electrical resistivities of Bi-doped and undoped Mg_2Si as a function of temperature.

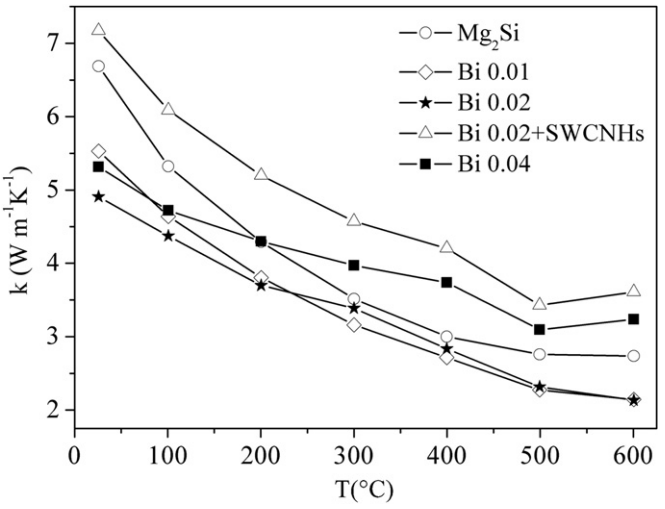

Fig. 8. Thermal conductivities of Bi-doped and undoped Mg_2Si as a function of temperature.

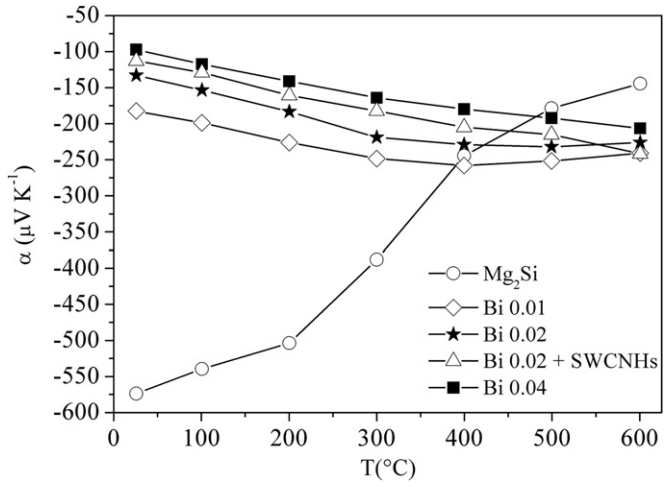

Fig. 7. Seebeck coefficients of Bi-doped and undoped Mg_2Si as a function of temperature.

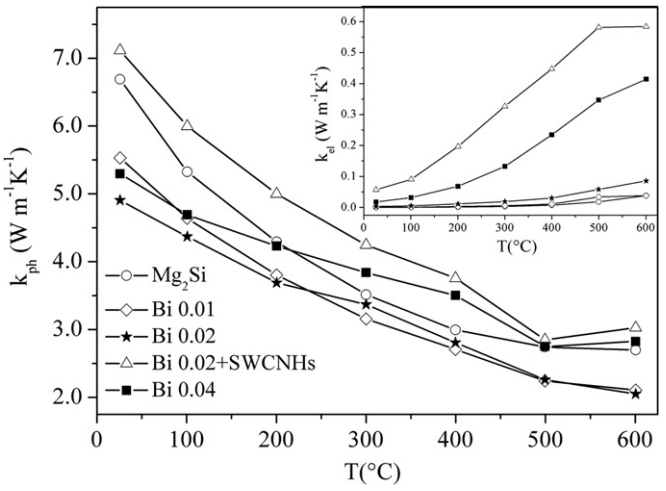

Fig. 9. Phonon (k_{ph}) and electrical (k_{el}) thermal conductivities of Bi-doped undoped Mg_2Si as a function of temperature.

Bi-doped materials. The absolute value of the Seebeck coefficients decreased with increasing Bi doping due to an augment of intrinsic charge carrier concentration.

The thermal conductivities are reported in Fig. 8. It has been observed that both the grain size and probably the presence of MgO decreased the thermal conductivities of the undoped sample and of samples with $x=0.01$ and $x=0.02$. In particular, the undoped specimen thermal conductivity values were found to be between MgO free Mg_2Si and 35% mol MgO Mg_2Si values reported by Riffel [29]. The sample with SWCNHs added presented the higher values of thermal conductivity, probably due to the further aggregation of the carbon nanohorns, which promoted an increase of this parameter. The high thermal conductivity of $x=0.04$ sample could be explained by the presence of the Bi_2Mg_3 metallic phase, as assumed by Choi et al. [22].

The contributions of lattice (k_{ph}) and electronic (k_{el}) components on the thermal conductivity were also evaluated (Fig. 9). These components can be separated by the Wiedemann–Franz law ($k_{el}=L\sigma T$) where σ is the electrical conductivity and the Lorenz number L is assumed to be a constant ($L=2.45\times 10^{-8}\,V^2\,K^{-2}$). The electronic contribution, as the electrical conductibility, increased with the Bi amount. With the exception of $x=0.04$ and $x=0.02+$SWCNHs samples, the k_{ph} decreased with the Bi content augmenting, as expected for Bi creating large mass contrast which disrupts the phonon path [2]. In $x=0.04$ and $x=0.02+$SWCNHs samples the k_{ph} probably increased due to the role of the Bi_2Mg_3 secondary phase and possible carbon nanostructure aggregates.

Fig. 10 shows the temperature dependence of the figure of merit of undoped samples and Bi-doped samples. *ZT* increased with increasing temperature, as previously reported for these materials [22,23,26,30]. A maximum *ZT* value of 0.39 at 600 °C was obtained for $x=0.02$ Bi-doped silicide with the addition of SWCNHs. In fact, adding carbon nanostructures to powders resulted both in a considerable increase of electrical conductivity and in a slight increase of thermal conductivity, as discussed above. However, this *ZT* value is lower with respect to the literature data [23], likely due to the significant oxide presence.

4. Conclusions

This work reports the synthesis of nanostructured doped magnesium silicide, employing commercial Mg_2Si raw pieces as starting material. The nanostructuring processes resulted in a significant oxide presence. Moreover, the crystallite size increased

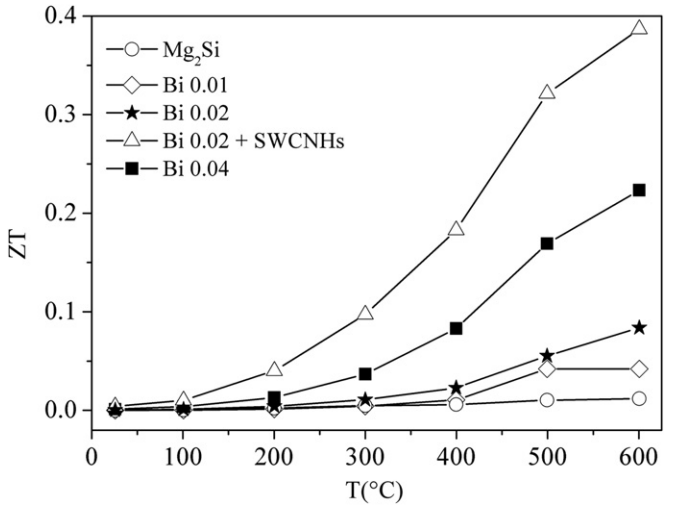

Fig. 10. Figure of merit of Bi-doped samples and undoped Mg_2Si as a function of temperature.

after each thermal process, highlighting the difficulty to preserve the original grain size in silicide materials.

Since the thermal treatments are required for doping the material and with the perspective of exploiting these materials in a high temperature range (up to 600 °C), it seems not necessary to synthesize powders with crystallite size lower than 200 nm, which is roughly the maximum value obtained after the several thermal cycles.

As to the oxide contamination, the effect on Seebeck coefficient resulted not significant, whilst thermal conductivities were only slightly influenced, but the samples presented higher electrical resistivities with respect to literature data.

The maximum *ZT* value of 0.39 at 600 °C was reached for the sample with $x=0.02$ Bi doped with the addition of SWCNHs. These carbon nanostructures increased considerably the electrical conductivity and slightly the thermal conductivity. The particular role of these carbon nanostructures will be the subject of further investigations in order to deep understand their effect on thermoelectric properties.

Acknowledgments

The authors are grateful to Dr Rosalba Gerbasi (CNR-ICIS) for XRD spectra and Mr Francesco Montagner (CNR-IENI) for the essential technical support.

This work has been funded by the Italian National Research Council—Italian Ministry of Economic Development II Agreement "Ricerca di sistema elettrico nazionale", Project "Materiali e tecnologie abilitanti per la ricerca di sistema elettrico".

References

[1] D.M. Rowe, CRC, Handbook on Thermoelectrics, Boca Raton, 1995.
[2] G.J. Snyder, E.S. Toberer, Nat. Mater. 7 (2008) 105–114.
[3] J. Tani, H. Kido, Intermetallics 15 (2007) 1202–1207.
[4] K. Nielsch, J. Bachmann, J. Kimling, H. Böttner, Adv. Energy Mater. 1 (2011) 713–731.
[5] B. Vining, Nat. Mater. 8 (2009) 83–85.
[6] J. Schilz, M. Riffel, K. Pixius, H.J. Meyer, Powder Technol. 105 (1999) 149–154.
[7] R.B. Song, T. Aizawa, J.Q. Sun, Mat. Sci. Eng. B: Solid 136 (2007) 111–117.
[8] J.-i. Tani, H. Kido, Intermetallics 16 (2008) 418–423.
[9] Y. Isoda, S. Tada, T. Nagai, H. Fujiu, Y. Shinohara, J. Electron. Mater. 39 (2010) 1531–1535.
[10] T. Sakamoto, T. Iida, S. Kurosaki, K. Yano, H. Taguchi, K. Nishio, Y. Takanashi, J. Electron. Mater. 40 (2011) 629–634.
[11] L.D. Hicks, M.S. Dresselhaus, Phys. Rev. B 47 (1993) 12727–12731.
[12] T. Sakamoto, T. Iida, A. Matsumoto, Y. Honda, T. Nemoto, J. Sato, T. Nakajima, H. Taguchi, Y. Takanashi, J. Electron. Mater. 39 (2010) 1708–1713.
[13] N. Gothard, J.E. Spowart, T.M. Tritt, Phys. Status Solidi A 207 (2010) 157–162.
[14] S. Iijima, M. Yudasaka, R. Yamada, S. Bandow, K. Suenaga, F. Kokai, K. Takahashi, Chem. Phys. Lett. 309 (1999) 165–170.
[15] S. Iijima, Physica B 323 (2002) 1–5.
[16] A. Izadi-Najafabadi, T. Yamada, D.N. Futaba, M. Yudasaka, H. Takagi, H. Hatori, S. Iijima, K. Hata, ACS Nano 5 (2011) 811–819.
[17] S. Battiston, M. Bolzan, S. Fiameni, R. Gerbasi, M. Meneghetti, E. Miorin, C. Mortalò, C. Pagura, Carbon 47 (2009) 1321–1326.
[18] S. Battiston, M. Minella, R. Gerbasi, F. Visentin, P. Guerriero, A. Leto, G. Pezzotti, E. Miorin, M. Fabrizio, C. Pagura, Carbon 48 (2010) 2470–2477.
[19] C. Pagura, S. Barison, S. Battiston, M. Schiavon, Anaheim, CA (2010) 289–291.
[20] L. Lutterotti, S. Mattheis, H.R. Wenk, ICOTOM-12 (1999) 1599.
[21] S. Boldrini, A. Famengo, S. Barison, In Preparation.
[22] S.-M. Choi, K.-H. Kim, I.-H. Kim, S.-U. Kim, W.-S. Seo, Curr. Appl Phys. 11 (2011) S388–S391.
[23] J.-i. Tani, H. Kido, Physica B 364 (2005) 218–224.
[24] W. Luo, M. Yang, F. Chen, Q. Shen, H. Jiang, L. Zhang, Mat. Sci. Eng. B: Adv. 157 (2009) 96–100.
[25] M. Yang, W. Luo, Q. Shen, H. Jiang, L. Zhang, Adv. Mat. Res. 66 (2009) 17–20.
[26] J.Y. Jung, I.H. Kim, Electron. Mat. Lett. 6 (2010) 187–191.
[27] S.W. You, K.H. Park, I.H. Kim, S.M. Choi, W.S. Seo, S.U. Kim, J. Electron. Mater. (2011) 1–5.
[28] S.-W. You, I.-H. Kim, Curr. Appl Phys. 11 (2011) S392–S395.
[29] M. Riffel, J. Schilz, ICT '97, 1997, pp. 283–286.
[30] T.J. Zhu, Y.Q. Cao, Q. Zhang, X.B. Zhao, J. Electron. Mater. (2009) 1–6.